Clinically compliant enrichment of human pluripotent stem cell-derived islets

Rajaei, B.; Garcia, A.M.; Juksar, J.; Doppenberg, J.B.; Paz-Barba, M.; Boot, F.; ... ; Carlotti, F.

CELL MANUFACTURING

Clinically compliant enrichment of human pluripotent stem cell–derived islets

Bahareh Rajaei[1], Amadeo Muñoz Garcia[1], Juri Juksar[1], Jason B. Doppenberg[2], Miriam Paz-Barba[1], Fransje Boot[1], Willemijn de Vos[1], Aat A. Mulder[3], Ferdy Lambregtse[1], Lizanne Daleman[1], Anne E. de Leeuw[1], Maaike C. Nieveen[1], Marten A. Engelse[1], Ton Rabelink[1], Eelco J. P. de Koning[1], Françoise Carlotti[1]*

Human pluripotent stem cell–derived islet (SC-islet) transplantation is a promising β cell replacement therapy for patients with type 1 diabetes, offering a potential unlimited cell supply. Yet, the heterogeneity of the final cell product containing non–target cell types has relevant implications for SC-islet function, transplant volume, and cell product safety. Here, we present a clinically compliant, full three-dimensional differentiation protocol that includes a purification step of endocrine cell–rich clusters, relying on the principle of isopycnic centrifugation (density gradient separation). Enriched SC-islets displayed signs of functionality in vitro and in vivo. In contrast with antibody-based single-cell sorting approaches, this method does not destroy the islet cytoarchitecture associated with alterations of islet function and cell loss. Furthermore, it is fast, is easily scalable to large cell volumes, and can be applied during cell manufacturing. This method may also contribute to the generation of improved cell-based therapies for regenerative medicine purposes beyond the SC-islet field.

INTRODUCTION

The progressive loss of insulin-producing β cells is a hallmark of type 1 diabetes, an autoimmune condition resulting from a combination of genetic and environmental factors. An insufficient functional β cell mass leads to an elevation of the blood sugar concentration (hyperglycemia), which can lead to ketoacidosis and death if left untreated. Transplantation of exogenous β cells to replace dead or dysfunctional endogenous β cells represents a potential functional cure, allowing proper control of blood glucose. Now, allogeneic pancreas and isolated islet transplantations are the two available options for cell replacement therapy (*1*, *2*). However, widespread implementation of this approach is hampered by a shortage of organ donors and the requirement for lifelong systemic immunosuppressive therapy.

Human pluripotent stem cells, including both human embryonic stem cells and human induced pluripotent stem cells (hiPSCs), constitute a virtually unlimited source of cells for islet replacement therapy. In an attempt to develop an off-the-shelf supply of β cells for transplantation, several multistage protocols have been developed to convert pluripotent stem cells into stem cell–derived islet (SC-islet) cells containing β cells in vitro (*3*–*5*), with recent advances leading to the generation of glucose-responsive insulin-secreting cells in a two-dimensional (2D) (*6*), combined 2D/3D (*7*–*9*), or full 3D culture system (*10*–*12*). Clinical studies have started using an earlier stage cell product (pancreatic endoderm) (*13*) and SC-islets (*14*). Clinical cell replacement therapies should involve fully defined and animal component–free processes to strictly meet the Good Manufacturing Practice (GMP) standards (*15*). In addition, 3D culture systems are more suitable for manufacturing large numbers of SC-islets for clinical application.

Despite major improvements in differentiation protocols, one of the main challenges for the field of stem cell–derived cell replacement therapies is the heterogeneity of the final cell product, defined as the presence of non–target cells after directed differentiation (*16*, *17*). Also for the generation of SC-islets, it is currently impossible to avoid the presence of non–islet cells in the final cell product (*10*, *18*). This is partly due to a limited knowledge of human islet developmental biology. A strategy to enrich for the target cells as the last step of the manufacturing process will increase efficiency while lowering the transplant volume, resulting in the generation of a potentially safer cell product.

To date, enrichment methods mainly rely on the use of specific cell surface markers for antibody-based sorting of subpopulations of interest and require the dissociation of cell clusters to single cells to specifically sort the target population (*10*, *19*–*31*). These procedures cause major cell loss and increase the risk of cellular stress in the remaining cells. In addition, the risk of contamination is enhanced because of additional manipulations. Furthermore, all of these strategies will disrupt the specific organization between the different islet cell types present in the endocrine cell–rich clusters, whereas the spatial arrangement and communication by paracrine signaling are known to substantially influence β cell function (*32*–*35*). Hence, developing a purification method that maintains their cytoarchitecture and composition will be beneficial for the preservation of β cell survival and function. Here, we present an easily scalable and clinically compliant method to enrich for endocrine cell–rich clusters, generated using a GMP-compliant, full 3D suspension differentiation protocol.

RESULTS

SC-islets are heterogeneous in cell composition for target endocrine cells and non–target cells

To develop a scalable, full 3D suspension, and GMP-compliant protocol for clinical application, we devised a seven-stage (~30-day) differentiation protocol based on earlier protocols (*8*–*10*) and applied

[1]Department of Internal Medicine, Leiden University Medical Center, Leiden 2333ZA, Netherlands. [2]LUMC Transplant Center, Leiden University Medical Center, Leiden 2333ZA, Netherlands. [3]Department of Cell and Chemistry Biology, Electron Microscopy Facility, Leiden University Medical Center, Leiden 2333ZA, Netherlands.
*Corresponding author. Email: f.carlotti@lumc.nl

GMP standards (fig. S1A): Cells were expanded and differentiated under defined antibiotic-free and xeno-free conditions (no fetal bovine serum or Matrigel was used). The protocol was optimized using the (research-grade) embryonic stem cell line HUES8 (*36*) and was applied on more lines including the clinical-grade RC9 embryonic stem cell line (*37*) as well as clinical-grade iPSC lines recently generated at our institute (*38*, *39*). Stage 7 cell products (SC-islets) consist of endocrine cell–rich [dithizone (DTZ) staining–positive] clusters and endocrine cell–poor clusters (Fig. 1A). SC-islets generated from HUES8 and RC9 cell lines contained on average 56.4 ± 5.0% SC-β cells (C-peptide–expressing cells), 8.5 ± 1.3% SC-α cells [glucagon (GCG)–expressing cells], and 5.5 ± 0.9% double-positive cells, expressing both C-peptide and GCG. A total of 21.1 ± 4.9% of the cells was double positive for C-peptide and NKX6.1 (Fig. 1B). The SC-β cells (C-peptide–expressing cells) showed expression of the key transcription factors NKX6.1, PDX1, and NEUROD1, whereas only rare β cells were positive for the maturity marker MAFA (Fig. 1C). The differentiation efficiency was comparable in three iPSC lines (fig. S1B). In addition, we found 8.6 ± 1.3% somatostatin-positive cells and 16.5 ± 4.2% SC-EC (enterochromaffin: SLC18A1-expressing cells) as non–islet endocrine cells as assessed by immunostaining (fig. S1, C and D).

Ultrastructure analysis by electron microscopy revealed that SC-β cells displayed endocrine granules, 200 to 300 nm in diameter, with an electron-dense core surrounded by a less dense halo, indicating some degree of maturity. Immunogold labeling for C-peptide validated the presence of insulin granules within SC-β cells (Fig. 1D).

SC-islets show limited glucose-stimulated C-peptide secretion capacity

A key feature of mature β cells is their capacity to respond to a glucose challenge by increasing insulin (or its by-product C-peptide) secretion, which returns to basal secretion upon subsequent exposure to a low glucose concentration. We evaluated SC-islet function in parallel to primary human donor islets obtained through our human islet isolation facility. The human C-peptide contents in SC-islets were 179.1 ± 42 (ng) per DNA (μg) (HUES8, $n = 11$) and 25.6 ± 14 (ng) per DNA (μg) (RC9, $n = 9$), whereas it was 899.5 ± 173.1 (ng) per DNA (μg) in donor islets ($n = 10$) (Fig. 1E). Upon static glucose stimulation, the stimulation indices (ratio of stimulated C-peptide to basal C-peptide) of SC-islets were 1.2 ± 0.5 (HUES8) and 1.6 ± 1.2 (RC9), whereas donor islets treated in parallel showed a stimulation index of 4.5 ± 3.1 (Fig. 1, F and G). The stimulation index of primary human donor islets is highly variable between islet cell preparations from different donors depending on a variety of circumstances including donor characteristics, ischemia time, culture duration, and aspects related to the isolation procedure as we previously reported (*40*).

In dynamic perifusion assays, SC-β cells showed a statistically significant ($P = 0.031$) response to glucose with a stimulation index of 1.9 ± 0.5 in the first 5 min after exposure to high glucose concentration (fig. S1E). Exposure to KCl, which depolarizes the cell membrane, resulted in a 12.6 ± 7.3–fold increase in C-peptide secretion compared with the baseline.

Functional adult islets are also characterized by increased mitochondrial respiration upon a glucose stimulus, which is associated with glucose-stimulated insulin secretion and indicates metabolic coupling to insulin release. We found an increase in the oxygen consumption rate (OCR) that was glucose dependent in primary donor islets, although responses were variable and often absent in SC-islet batches (Fig. 1, H and I). Maximal respiratory capacity and spare capacity were also reduced in RC9-islets compared with primary islets, indicating a lesser ability of SC-islet cells to produce adenosine 5′-triphosphate (ATP) at their maximum rate and a reduced response to increased energy demand and stress. Together, SC-islets generated by this GMP-compliant, full 3D differentiation protocol showed insulin secretory capacity, although to a reduced extent compared with primary islets.

SC-β cells display a transcriptional signature reminiscent of primary donor islet β cells

To obtain an in-depth characterization of SC-β cells, we performed single-cell RNA sequencing to compare their transcriptional profile with that of β cells from primary human islets (donor β cells). We first assessed the expression of selected β cell identity genes as defined by a previous study (*41*). We found that, despite some differences between the two cell lines, HUES8-β and RC9-β cells shared similarities in the expression of β cell identity genes and islet functionality genes to the donor β cells, including *INS*, *PDX1*, *NKX6.1*, *SLC30A8*, *ABCC8*, *PCSK1*, *ENO1*, *ENO1B*, *UCHL1*, *NEUROD1*, *NKX2.2*, *MNX1*, and *CDKN1C* (Fig. 2A and fig. S2A).

In addition, SC-β cells expressed genes involved in β cell function including glucose sensing and signaling (*ABCC8*, *KCNJ11*, *SLC2A1*, *CANA1C*, *SLC30A8*, *GRN*, and *CAMK2N1*) and exocytosis (*VAMP2*, *CDC42*, *STX1A*, *SNAP25*, and *STXBP1*) (Fig. 2, B and C). Also, expression of *SLC25A1*, which is responsible for transporting citrate across the inner mitochondrial membrane and is a key step in the tricarboxylic acid (TCA) cycle, in SC-β cells was similar to that in donor β cells (Fig. 2, C and D). However, SC-β cells displayed lower expression of some other genes associated with β cell maturation (*UCN3*, *MAFA*, and *SIX3*) and function (*ADCYAP1*, *VGF*, *KCNK3*, *G6PC2*, and *ABCC9*).

Last, genes associated with respiration in mitochondria, the electron transport chain complexes including *MT-ND3* (complex I), *SDHB* (complex II), *UQCRFS1* (complex III), *MT-CO1* (complex IV), *MT-ATP6* (complex V), and *CYCS* (cytochrome c), showed similar expression patterns in SC-β cells compared to donor β cells, indicative of functional mitochondria in SC-β cells (Fig. 2E and fig. S2, A and B), which is consistent with the mitochondrial oxygen consumption profile. Further analysis of hallmark genes related to oxidative phosphorylation and protein secretion, using the Molecular Signatures Database, confirmed the similarity between donor β cells and SC-β cells. Overall, this shows that the protocol generated insulin-producing cells with a transcriptional profile related to β cell identity and metabolism.

SC-β cells function in vivo after transplantation

To assess the capacity of SC-islets to function in vivo, we transplanted cell clusters under the kidney capsules of immunodeficient mice and subjected the mice to a glucose challenge at different time points posttransplantation (Fig. 3A). Stimulated human C-peptide was detectable from 14 days posttransplantation, indicating successful engraftment of the SC-islets. Human C-peptide secretion increased by 8.2- and 7.3-fold on day 90 compared with day 14 in HUES8- and RC9-islet cell transplants, respectively (Fig. 3, B and C). Furthermore, we observed a significant increase ($P = 0.02$) in human C-peptide released at 30 min post–glucose injection compared with basal secretion from day 90 posttransplantation onward (fig. S3, A to F). Immunostaining of the

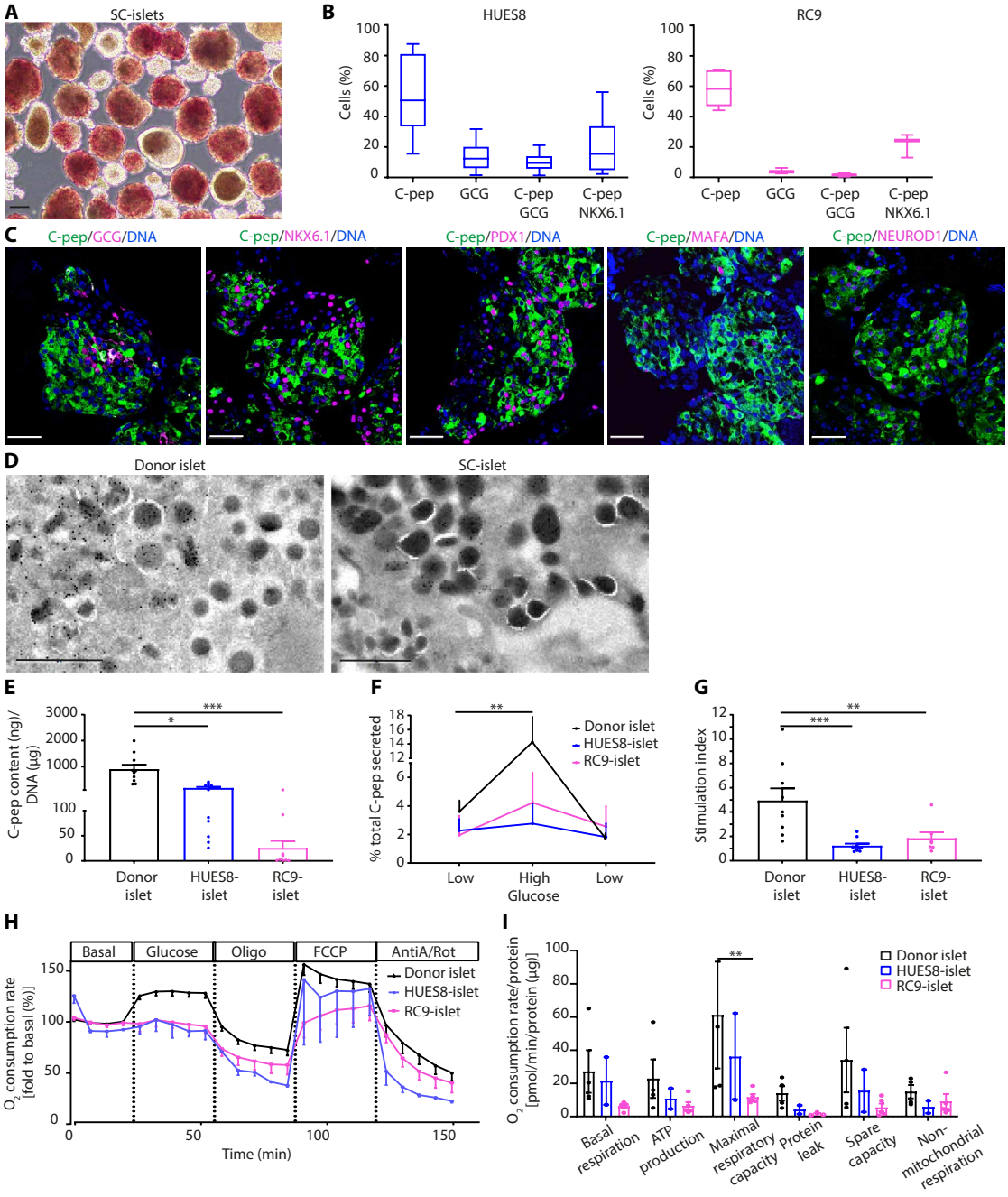

Fig. 1. Characterization of SC-islet composition and function. (**A**) Morphology of the cell clusters at stage 7 (scale bar, 100 µm). Endocrine cell–rich clusters are stained with DTZ. (**B**) Frequency of C-peptide, GCG-positive, bihormonal (C-peptide/GCG), and C-peptide/NKX6.1 cells in SC-islets derived from HUES8 ($n = 16$) or RC9 ($n = 7$) cells, as assessed by flow cytometry. Data are presented as a box plot, and the median is shown. (**C**) Immunostaining for C-peptide (green) and GCG, NKX6.1, PDX1, MAFA, or NEUROD1 (all in pink) of SC-islets. Scale bars, 50 µm. (**D**) Electron microscopy images of a donor islet β cell (left) and of a β cell from SC-islets (right) labeled with immunogold staining for C-peptide. Scale bars, 1 µm. (**E**) C-peptide content (ng) normalized to DNA content (µg) of SC-islet cells derived from HUES8 (HUES8-islet, $n = 10$), RC9 (RC9-islet, $n = 9$), or donor islets ($n = 10$). Kruskal-Wallis with Dunn's multiple comparison; significance versus donor islet, when indicated. (**F**) Glucose stimulated C-peptide secretion of donor islets ($n = 10$) and SC-islets derived from HUES8 (HUES8-islet, $n = 10$) or RC9 (RC9-islet, $n = 9$) cells, normalized to the C-peptide content. Cell clusters were incubated at low glucose concentration (1.67 mM) and subsequently to high glucose concentration (20 mM) and to low glucose concentration (1.67 mM glucose) again. Two-way ANOVA with Dunnett's multiple comparison tests; significance versus basal secretion at low glucose concentration, when indicated. (**G**) Stimulation index (fold change of C-peptide secretion at high glucose concentration over the first low glucose concentration) of donor islets ($n = 10$) and SC-islets derived from HUES8 (HUES8-islet, $n = 10$) or RC9 (RC9-islet, $n = 9$) cells; one-way ANOVA; significance versus donor islets, when indicated. (**H**) OCR of donor islets ($n = 4$) and SC-islets derived from HUES8 (HUES8-islet, $n = 2$) or RC9 (RC9-islet, $n = 5$) cells in response to 20 mM glucose (glucose), oligomycin (oligo) (5 µM), FCCP (carbonyl cyanide p-trifluoromethoxyphenylhydrazone) (4 µM), and rotenone/antimycinA (AntiA/Rot) (1 µM/1 µM). Data are normalized to the basal respiration and presented as percentage. (**I**) Mitochondrial properties indicating OCR normalized to protein content of donor islets ($n = 4$) and SC-islets derived from HUES8 (HUES8-islet, $n = 2$) or RC9 (RC9-islet, $n = 5$) cells. Two-way ANOVA with Holm-Šidák multiple comparisons test. All data are means ± SEM. $^*P < 0.05$, $^{**}P < 0.01$, and $^{***}P < 0.001$.

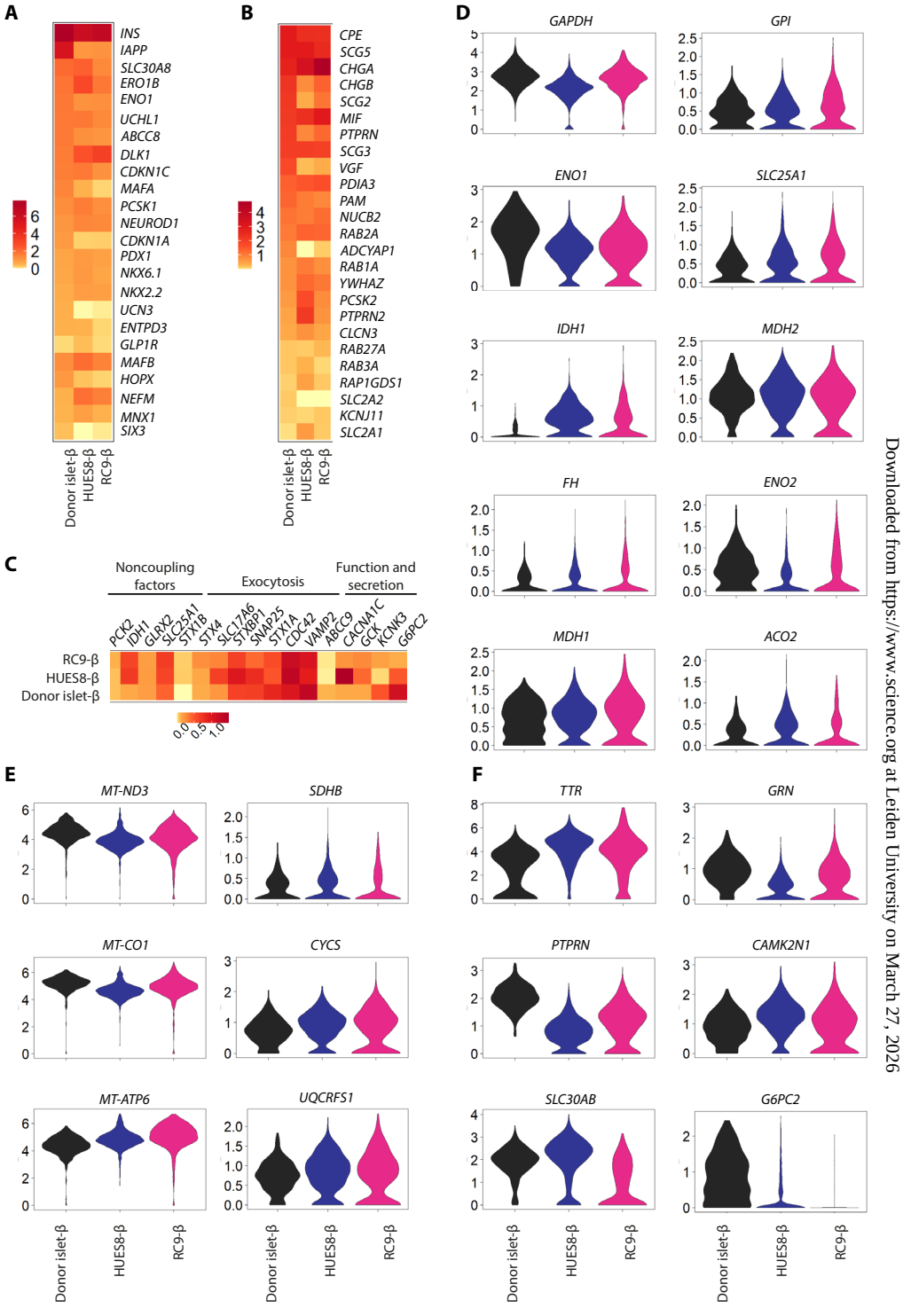

Fig. 2. Single-cell transcriptomic profiling of SC-β cells. (**A** to **C**) Heatmap showing the mean expression of selected genes associated with β cell identity and maturation (*41*) (A), β cell metabolic sensing and signaling including glucose sensing [adapted from (*8*, *10*)] (B), and β cell function and secretion, exocytosis, and noncanonical factors [adapted from (*8*, *10*)] (C) in β cells from donor islets (donor islet-β, $n = 3$) and SC-β cells derived from HUES8 (HUES8-β, $n = 2$) or RC9 (RC9-β, $n = 3$) cells. (**D** to **F**) Violin plot representing the expression of selected genes [from (B) and (C)] related to glycolysis and TCA cycle (D), oxidative phosphorylation (E), and insulin secretion (F) in β cells from donor islets ($n = 3$) and SC-β cells derived from HUES8 ($n = 2$) or RC9 ($n = 3$) cells.

grafts validated the presence of SC-islets containing C-peptide–positive β cells and GCG-expressing α cells (Fig. 3D). Bihormonal cells (coexpressing both C-peptide and GCG) were only rarely found.

In summary, SC-islets generated from this protocol engrafted well in vivo and showed evidence of functional maturation of SC-β cells over time. This highlights the potential of SC-islets as surrogate cells for the development of cell-based replacement therapies.

Enrichment of SC-islets by a clinically applicable density gradient separation

Next, we reasoned that our protocol could be further improved by adding a last step to enrich the final cell product for islet cell–rich clusters to generate a product of lower volume and, therefore, higher process efficacy. Building from our expertise in clinical islet isolation, during which digestion of pancreatic tissue is followed by a

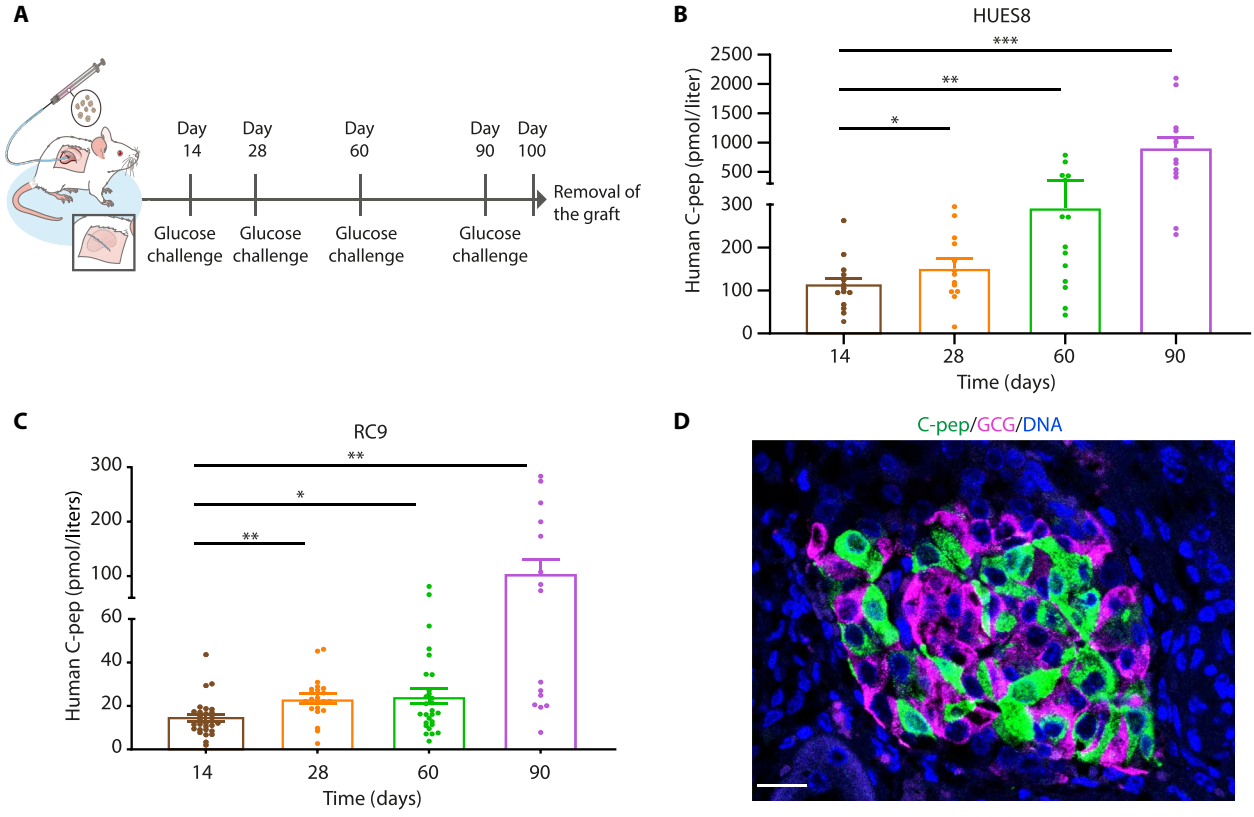

Fig. 3. Engrafted SC-islets in immunodeficient mice. (**A**) Schematic representation of the in vivo experimental setup indicating the time points at which glucose challenges were performed. (**B** and **C**) Maximum stimulated human C-peptide concentration in mice engrafted with SC-islets derived from HUES8 [(B); day 14 ($n = 14$), day 28 ($n = 14$), day 60 ($n = 14$), and day 90 ($n = 13$)] and RC9 [(C); day 14 ($n = 29$), day 28 ($n = 29$), day 60 ($n = 28$), and day 90 ($n = 15$)] cells; mixed-effect analysis using Dunnett's multiple comparison; significance compared with day 14, when indicated. All data are means ± SEM. *$P < 0.05$, **$P < 0.01$, and ***$P < 0.001$. (**D**) Immunostaining for C-peptide (green) and GCG (pink) of SC-islets at 100 days postengraftment. Scale bar, 20 μM.

separation of the donor islets from exocrine tissue using isopycnic centrifugation (density gradient separation), we hypothesized that endocrine cell–rich clusters would have a different density from the (non–target) endocrine cell–poor clusters and could therefore be separated from each other using a similar separation method.

We established a linear (continuous) density gradient using clinically applicable reagents [University of Wisconsin (UW) solution, a commonly used organ preservation solution, and iobitridol (Xenetix), a radiocontrast agent] ranging in density between 1.045 and 1.100 g/ml (Fig. 4, A and B, and table S1). The gradient was validated by assessing the density of each fraction using a density meter (Fig. 4B). After centrifugation, the gradient was divided into seven fractions of similar (gradient medium) volume. We found that cell viability was not affected, as assessed up to 10 days post–density gradient separation (Fig. 4C).

We used DTZ, a zinc-binding dye, to identify the endocrine cell–rich clusters (Fig. 4D). We then assessed the frequency of DTZ-positive clusters (fig. S4A) and quantified the amount of tissue obtained per fraction (fig. S4B). The normalized purity of each fraction showed that fractions 2 to 5 contained the most endocrine cell–rich clusters (Fig. 4E). These findings were confirmed by total C-peptide content (fig. S4C). For the subsequent experiments, we pooled fractions 2 to 5 together in a so-called "enriched SC-islet" fraction that consisted of 92.8 ± 1.5% DTZ-positive tissue (Fig. 4F). C-peptide content analysis indicated that enriched SC-islets contained 67.6 ± 3.6% C-peptide (fig. S4D). A similar range of purity was obtained when assessed on the basis of the frequency of DTZ-positive clusters in the enriched fractions compared with nonpurified cells (fig. S4E). Overall, cell clusters from the enriched SC-islet fraction (pooled fractions 2 to 5) displayed a twofold higher C-peptide content as compared with those of the "depleted SC-islet" fraction (fractions 1, 6, and 7 pooled together) (fig. S4, C and D), which was consistent across cell lines RC9, HUES8, and LUMC iPSC1 (fig. S4F).

The amount of tissue collected in the enriched SC-islet fraction contained 82.2 ± 3.6% of the initial tissue mass, indicating that the tissue volume for transplantation was reduced by 17.8 ± 3.6% (fig. S4G). Cell clusters from enriched SC-islets were mostly present at a density of 1.053 to 1.088 g/ml, which is within the range of primary human islet density [1.067 to 1.087 g/ml (*42*)].

Further characterization by immunostaining confirmed the enrichment of synaptophysin (SYP; endocrine)–, C-peptide–, and GCG-positive cell clusters in the enriched SC-islet fraction, whereas the depleted SC-islet fraction showed an enrichment in CK19-positive (ductal) cell clusters (Fig. 4G and fig. S4, H and I). Transmission electron microscopy and immunogold labeling validated the presence of insulin granules in cells from enriched SC-islets (Fig. 4H).

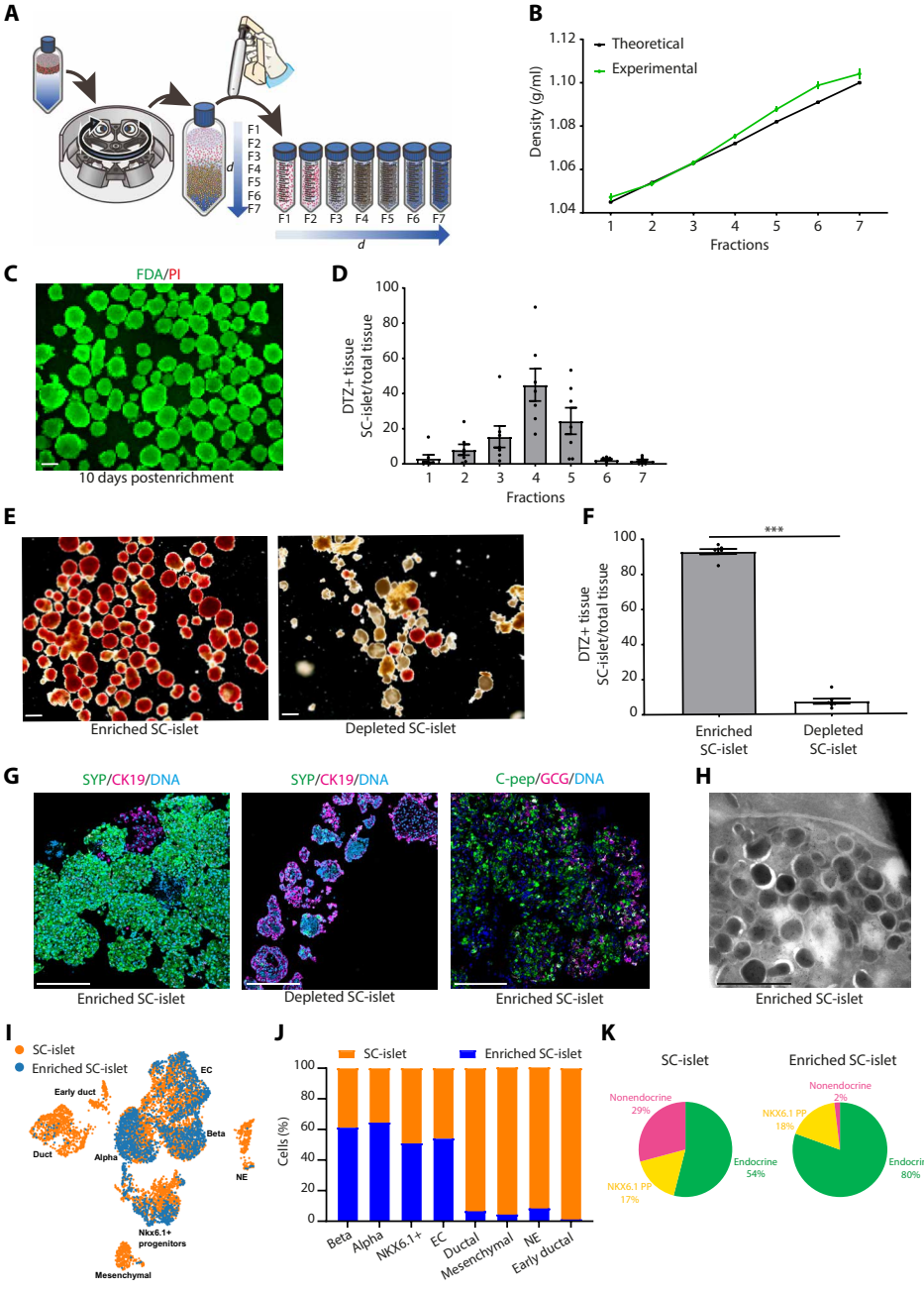

Fig. 4. Enrichment of SC-islets by density gradient separation. (**A**) Schematic representation of the density gradient separation method. A linear density gradient was first prepared. SC-islet cell clusters were then loaded on top of the gradient medium in a 50-ml conical tube that was subsequently subjected to centrifugation. Next, seven fractions of a similar volume were collected in new 50-ml tubes and further assessed for their composition. (**B**) Linear density (g/ml) gradient as calculated (theoretical) for each fraction and experimentally validated by measurement using a density meter. (**C**) Representative image of a viability assay of cell clusters stained with fluorescein diacetate (FDA; live cells, green)/propidium iodide (PI; dead cells, red) at 10 days post–density gradient separation. Scale bar, 200 μm. (**D**) Representative images of DTZ staining of enriched SC-islet (left) and depleted SC-islet (right) fractions. Scale bars, 200 μm. (**E**) Proportion of DTZ-positive tissue in each fraction, normalized to the amount of tissue (DNA content per fraction). Data were collected from seven independent experiments [HUES8 ($n = 3$) and LUMC iPSC1 ($n = 4$)]. (**F**) Proportion of DTZ-positive tissue in enriched SC-islets (pooled fractions 2 to 5) and depleted SC-islets (fractions 1, 6, and 7), normalized to the amount of tissue (DNA content per fraction). Data were collected from seven independent experiments [HUES8 ($n = 3$) and LUMC iPSC1 ($n = 4$)]. One-tailed Mann-Whitney test. (**G**) Representative images of immunostaining for SYP (endocrine cells; green) and KRT19 (ductal cells; pink) in enriched SC-islets (left) and depleted SC-islets (middle) and representative image of immunostaining of C-peptide (green) and GCG (pink) in enriched SC-islets (right); scale bars, 200 μm. (**H**) Electron microscopy image of a β cell from enriched SC-islets labeled with immunogold staining for C-peptide. Scale bar, 1 μm. (**I**) UMAP (uniform manifold approximation and projection) plot indicating the cell populations in SC-islets before (SC-islet) and after (enriched SC-islet) density gradient separation (HUES8, $n = 1$). (**J**) Frequency of the cell types present in SC-islets before (SC-islet) and after (enriched SC-islet) enrichment (HUES8, $n = 1$). (**K**) Frequency of the endocrine and nonendocrine cells in SC-islets before (SC-islet) and after (enriched SC-islet) enrichment (HUES8, $n = 1$).

Last, we performed single-cell transcriptomics showing the identity of the cell types present in the preparation before versus after enrichment (Fig. 4, I to K, and fig. S4, J and K). These include islet cells, exocrine cells, and neuroendocrine cells (GAP43$^+$ NE) but also non–target cell populations such as enterochromaffin cells and mesenchymal cells, in line with findings from others (*8*, *10*, *43*). These data, although from one experiment, confirmed an enrichment in endocrine cells from 54 to 80% post–density gradient separation and a strong reduction in nonendocrine (early ductal, ductal, mesenchymal, and neuroendocrine) cells from 29 to 2% post–density gradient separation.

The expression of identity and functionality genes in SC-β cells remained stable after enrichment (fig. S4, L to N). In addition, genes associated with respiration in mitochondria, the electron transport chain complexes including *MT-ND3* (complex I), *SDHB* (complex II), *UQCRFS1* (complex III), *MT-CO1* (complex IV), *MT-ATP6* (complex V), and *CYCS* (cytochrome c), remained unaffected (fig. S4, O to Q).

Enriched SC-islets are functional in vitro and in vivo

Next, we assessed the functionality of the purified cell clusters using a dynamic glucose-stimulated C-peptide secretion test. SC-islets and enriched SC-islets showed a comparable stimulation index after exposure to high glucose concentration (Fig. 5A). Upon exposure to KCl, which depolarizes the cell membrane, enriched SC-islets showed a 26.1 ± 18.6–fold increase in C-peptide concentration, which was two times higher, compared with SC-islets before enrichment (12.8 ± 5.9) (Fig. 5B). This reflects the higher C-peptide content observed as shown in Fig. 5C.

Mitochondrial function was unaltered in ATP production, proton leak, spare capacity, and nonmitochondrial respiration after the purification procedure. However, basal respiration and maximum respiratory capacity were higher in enriched SC-islets (Fig. 5D), indicating that these cells are more metabolically active and potentially better equipped to handle energy demands. Cell clusters from enriched SC-islets showed a low and stable intra-islet calcium activity ($[Ca^{2+}]_i$) at low glucose concentration compared with SC-islets and increased frequency in cells displaying a glucose-induced calcium response, thereby indicating an enrichment in functional endocrine cells (Fig. 5E).

Last, clusters from the enriched SC-islet fraction engrafted well in vivo and were functional up to 6 months posttransplantation (Fig. 5F and fig. S5, A to D). Mice transplanted with SC-islets and enriched SC-islets showed a more rapid glucose clearance over time (fig. S5, E to H) and displayed lower nonfasting blood glucose concentrations, reaching the human glycemic set point (~5 mM) from 3 months onward (fig. S5I), indicating the improved functionality of the engrafted SC-β cells. We did not observe severe hypoglycemia during welfare assessments in a follow-up period up to 6 months posttransplantation, indicating that the secretion of C-peptide was regulated.

Histological analyses at the time of transplantation (fig. S5J) and after 170 days confirmed the enrichment in SYP (endocrine), C-peptide, and GCG-positive cells in the graft as well as the reduced frequency of CK19 (ductal) cells and associated cystic structures (Fig. 5G). Enterochromaffin cells remained present in grafts postenrichment (fig. S5K). We also observed enhanced expression of the β cell maturity marker MAFA posttransplantation, providing additional evidence for maturation of the graft (fig. S5L).

Density gradient separation was successfully performed in two human embryonic stem cell lines (HUES8 and RC9) and three hiPSC lines, demonstrating the robustness of the separation method. Together, these data validate density gradient separation as a GMP-compliant purification method to enrich SC-islet preparations for endocrine cell–rich clusters in the final cell product while showing no adverse effect on the biological activity of the cells.

DISCUSSION

Here, we present a GMP-compliant, full 3D suspension differentiation protocol for SC-islets with enrichment in endocrine cell–rich clusters by density gradient separation for clinical application. SC-β cells resulting from this protocol displayed key genes associated with β cell identity and function. Yet, in accordance with the literature (*11*), these cells mostly lacked the expression of maturity genes such as MAFA and showed limited glucose-dependent insulin secretion and oxygen consumption in vitro because of a glycolytic bottleneck, inhibiting glucose metabolism and sensing in SC-β cells. Nevertheless, our enriched SC-islets engrafted properly and matured further after transplantation.

Despite major progress in differentiation protocols, one of the main challenges for manufacturing hiPSC-based cell replacement therapies is the elimination of non–target cells in the final cell product, which is relevant in the context of (reduced) transplant volume, efficacy, and safety. We found that the final cell product generated from a full 3D suspension differentiation protocol produced endocrine cell–rich clusters and endocrine cell–poor clusters. Building on the knowledge and experience (since 2007) of our center in islet isolation procedures from primary human pancreatic tissue (*42*, *44*), we developed a GMP-compliant purification technique relying on the principle of density gradient separation. This method enabled us to enrich SC-islet preparations in endocrine cell–rich clusters on the basis of the density of the cell cluster, regardless of its size. Cell cluster size only influences the rate at which cell clusters move until their density is the same as the surrounding gradient medium.

This method enabled enrichment in endocrine cells and depletion of nonendocrine cells, leading to a more consistent cell product with reduced non–target cells as shown by various assays including single-cell transcriptomics before versus after enrichment, although single-cell transcriptomics was limited to one experiment in this study. The depletion in ductal and other non–target cells largely reduced the frequency of nonendocrine structures often observed with such a protocol upon transplantation (*45*, *46*). Yet, further long-term safety in vivo studies are needed to reach a first-in-human trial.

Cell viability and functionality were unaffected given that the procedure does not disturb cell cluster cytoarchitecture, with cell-cell contacts well known to play a critical role in the maintenance of β cell health and function in the context of primary islets (*32*–*35*). This is in contrast with previously reported purification methods that rely on the dissociation of the cell product to single cells, combined with antibody-based detection of the target cell type by fluorescence-activated cell sorting or magnetic-activated cell sorting technologies (*10*, *19*–*31*).

The current differentiation protocols typically generate a proportion of enterochromaffin-like cells as reported by Schmidt *et al.* (*43*). Our current density gradient separation method does not allow for separation of these cells from other endocrine islet cells. On the other hand, a recent study suggested that these cells resemble a serotonin-producing pre–β cell population present in the fetal pancreas, suggesting a pancreatic rather than intestinal origin (*47*). More studies are needed to clarify further the origin of these cells.

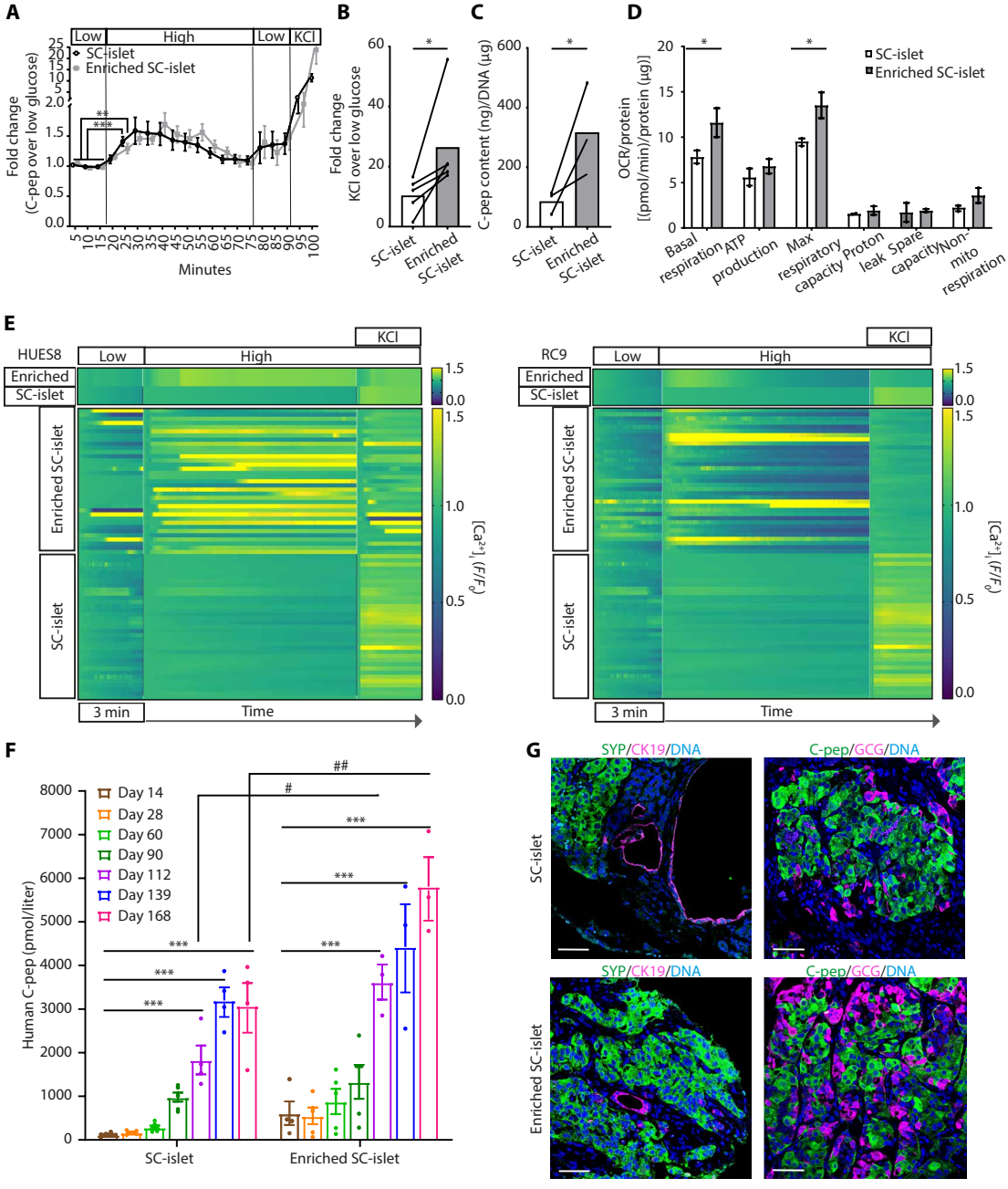

Fig. 5. Enriched SC-islets are functional in vitro and in vivo. (**A**) Stimulation index (fold change of C-peptide secretion at high glucose concentration over the average of basal secretion in the last three time points of first low glucose concentration) of SC-islets (nonpurified) and enriched SC-islets in five independent experiments [HUES8 ($n = 2$) and LUMC iPSC1 ($n = 3$)] during dynamic perifusion with 1.67 to 20 mM glucose and 30 mM KCl. Paired one-tailed Student's *t* test; significance versus average of three time points at first low glucose concentration, when indicated. **(B** and **C)** Fold secretion of C-peptide concentration in KCl over first low glucose concentration (B) and C-peptide content (ng) normalized to DNA content (µg) (C) of SC-islets (nonpurified) and enriched SC-islets in five independent experiments [HUES8 ($n = 2$) and LUMC iPSC1 ($n = 3$)] and three independent experiments [HUES8 ($n = 1$) and LUMC iPSC1 ($n = 2$)], respectively. For (B), one-tailed Wilcoxon test; for (C), paired one-tailed Student's *t* test; significance versus SC-islet (nonpurified), when indicated. (**D**) OCR normalized to total protein content in enriched SC-islets (fraction 4) compared with nonpurified SC-islets, indicating different aspects of mitochondrial function; two independent experiments [HUES8 ($n = 1$) and RC9 ($n = 1$)]. Two-way ANOVA with Holm-Šidák multiple comparisons. Significance compared with nonpurified cells, when indicated. (**E**) Intracellular calcium ($[Ca^{2+}]$) recordings upon incubations of enriched SC-islets or SC-islets derived from HUES8 ($n = 1$, left) and RC9 ($n = 1$, right) cells with 1.67 and 20 mM glucose or 30 mM KCl. Relative fluorescence changes as a function of time, showing the mean of cell response (top heatmap) and each line representing one cell (bottom heatmap). (**F**) Maximum stimulated human C-peptide concentration in mice engrafted with SC-islets (nonpurified) or enriched SC-islets derived from HUES8 (two independent experiments, $n = 6$ mice per condition up to 100 days and 3 mice per condition up to 170 days). Mixed-effect analysis using Šidák's multiple comparisons test when comparing enriched SC-islets with SC-islets. Significance compared with SC-islets, when indicated. Mixed-effect analysis using Dunnett's multiple comparisons test when comparing days posttransplantation to day 14 within each group. Significance compared with day 14, when indicated. All data are means ± SEM. $^{*}P < 0.05$ or $^{\#}P < 0.05$, $^{**}P < 0.01$ or $^{\#\#}P < 0.01$, and $^{***}P < 0.001$ or $^{\#\#\#}P < 0.001$. (**G**) Representative immunostainings for SYP (endocrine cells; green), KRT19 (ductal cells; pink) (left), C-peptide (green), and GCG (pink) (right) in SC-islets before (top) and after enrichment (bottom) at 170 days postengraftment. Scale bar, 50 µM.

There are limitations to this study. First, although we tested the density gradient separation method in SC-islets generated from five pluripotent stem cell lines, we observed some variability among experiments. This indicates that the optimal fractions for enriched SC-islets differ between lines, probably because of the variation in the density of SC-islets, which is influenced by the degree of maturation of the cells. Hence, the selection of fractions should be adapted per line. Second, the functionality of enriched SC-islets was assessed upon glucose challenge after transplantation in normoglycemic animals; thus, it remains to be determined how enrichment will affect the therapeutic dose in a diabetic animal model.

Overall, we propose density gradient separation as a robust, easily scalable, and clinically applicable technique for effective purification of SC-islet preparations with endocrine cell–rich clusters. Enrichment of the endocrine populations in the final cell product is expected to improve transplantation efficacy and safety. Furthermore, we envision that this enrichment method can be applied to other pluripotent stem cell–based products beyond SC-islets.

MATERIALS AND METHODS

Study design

In this study, we used a full 3D suspension differentiation protocol that we complemented with an enrichment method for endocrine cell–rich clusters (target cells) based on density gradient separation. The protocol was applied on several human pluripotent stem cell lines, and the cell products were characterized by multiple assays including flow cytometry, immunostaining, and single-cell transcriptomics. Furthermore, we assessed the functionality of the SC-β cells in vitro by static or dynamic glucose-stimulated insulin secretion test, calcium assay, and mitochondrial respiration and in vivo upon transplantation in immunodeficient mice.

In vitro culture and differentiation of hiPSCs

Human embryonic stem cell lines RC9 and HUES8 were obtained from the Roslin Institute and WiCell, respectively. The hiPSC lines LUMC iPSC1, LUMC iPSC2, and LUMC iPSC3 (Lumc-Gmp-ipsc_donor-02 Line 1b/2/3) were generated in the GMP facility of our institute (*38*, *39*). A vial of these cells was subsequently transferred to a regular research lab and expanded further for use in this study. HUES8 cells were cultured on laminin 521 (Biolamina, LN521), and RC9 and LUMC iPSCs were cultured on vitronectin (Thermo Fisher Scientific, A14700)–coated plates in Essential 8 medium (Thermo Fisher Scientific, catalog no. A1517001) and passaged using Versene (Gibco, 15040-033). To prepare for the differentiation experiments, 70% confluent 2D culture flasks of hiPSCs were dissociated using Accutase (Stemcell Technologies, catalog no. 07920) and seeded in Essential 8 supplemented with 10 μM rho-associated kinase inhibitor (Y-27632; Stemcell Technologies, 72304) at a density of 0.5 million cells/ml in either a 125-ml disposable spinner flask (Corning; 3152) or 30-ml disposable bioreactor (ABLE Biott; ABBWVS03A-6) on a magnet stir plate set to 60 rpm in a 37°C incubator at 5% CO_2 and 100% humidity.

To start the differentiations, the medium was changed to D0 medium 48 hours postseeding. The differentiation was carried out using a multistage protocol and adapted from (*8*–*10*), culturing the cells in a 3D suspension culture system (disposable bioreactors) for the course of differentiation for about a month. We considered "GMP-compliant" reagents as those available as clinical grade, aiming for a process entirely animal component–free. All cultures including expansion and differentiation media were kept antibiotic-free to comply with GMP regulations. Experiments reported here have been performed with research-grade reagents. Complete medium formulations are available in table S2. Medium refreshments were performed daily throughout stages 1 to 5 and every other day in stages 6 and 7.

Primary human islets

Donor islets were obtained from cadaveric human organ donors. Human islet isolations were performed at our institute. Islets were used for research only if they could not be used for clinical purposes and if research consent was present, according to Dutch national laws. Islets were cultured in regular CMRL 1066 medium (5.5 mM glucose), supplemented with 10% human serum, 10 mM Hepes (Lonza, BEBP17-737E), 2 mM L-glutamine (Lonza, BEBP17-605E), nicotinamide (1.2 mg/ml; Apotheek AZL, 97996807), ciprofloxacin (20 μg/ml; Fresenius Kabi, 15999149), and gentamycin (50 μg/ml; Centrafarm b.v., RVG 57572) in platelet storage bags (Terumo BCT, 70030) at 37°C in a 5% CO_2-humidified atmosphere; the medium was refreshed the day after isolation and every two days thereafter. Donor islet purity and other characteristics are listed in table S3.

Transplantation studies

All animal experiments were approved by the animal welfare committee of the Leiden University Medical Center (project license number AVD11600202216416). Transplantations were performed in 5- to 12-week-old male (immunodeficient) NSG-RIP-DTR mice (*48*). Two to four animals settled per cage with unlimited access to food and water, subjected to a 12-hour light and 12-hour dark cycle. Briefly, SC-islets were implanted under the kidney capsule of mice. Animals were anesthetized with isoflurane inhalation. A small incision was made in the kidney capsule using a 27G needle tip, and a space was created between the kidney and the capsule. Cells were collected in a cannula and transplanted underneath the capsule using a Hamilton syringe. Body weight and nonfasted blood glucose values (from tail tip blood) were monitored twice weekly postsurgery. The functionality of SC-islets was assessed by performing a glucose challenge (intraperitoneal glucose tolerance test) at 14, 28, 60, and 90 days postsurgery. In addition, mice engrafted with enriched SC-islets were assessed up to 170 days posttransplantation. Briefly, blood samples were taken from the tail vein after 4 hours of fasting ($t = 0$). Glucose was administered (2 g/kg), and blood glucose values were tested at 15, 30, 60, and 120 min. Additional blood samples were taken at 30 and 60 min. The concentration of human C-peptide was tested on the blood plasma with a human ultrasensitive C-peptide ELISA (Mercodia, 10-1141-01). At the end of the experiments, animals were sacrificed and organs were harvested and fixed in 4% paraformaldehyde. Engrafted kidneys were further processed for histological analysis.

DTZ staining

Zinc-chelating dye DTZ (Sigma-Aldrich, D5130) stock solution was prepared with 50 mg of DTZ in 10 ml of NaOH and ethanol. The staining solution was mixed and filtered through a 0.45-μm nylon filter and then used as the DTZ working solution. The SC-islets were stained for 5 min in the DTZ solution. Then, SC-islets were rinsed three times with Dulbecco's phosphate-buffered saline and imaged with a light microscope (Olympus CKX53).

Density gradient separation method

SC-islets were cultured in islet medium with 5 mM glucose 24 hours before purification. A density gradient with a continuous linear slope was formed in a 50-ml tube. First, a high-density solution (1.100 g/ml) was made by mixing a clinically approved radiocontrast agent [iobitridol (Xenetix)]. A 7-ml layer of the high-density solution was loaded into the tube. Thereafter, a 35-ml linear gradient of varying density was created by mixing the high-density solution with the UW solution (1.045 g/ml) using computer-programmed peristaltic pumps [Maxiflow peristaltic pump (Lambda laboratories instruments, Prague, Czechia)]. Lastly, a layer of UW solution was loaded (table S1). Before purification, SC-islets were incubated in UW solution for 30 min at 4°C. Thereafter, cell clusters were gently loaded on top of the gradient. Then, SC-islets were centrifuged at 200*g* for 7 min with acceleration at 7*g* and deceleration at 3*g* at 4°C. Seven fractions of 7 ml of gradient medium were collected and distributed across 50-ml tubes. Cell clusters from each fraction were collected by passing through a cell strainer with a pore size of 0.45 μm and washed in islet medium to remove the gradient components (Xenetix and UW solutions). Then, the density of collected gradient medium was re-measured for validation by a density meter (Anton Paar, DMA-35 N). Subsequently, each fraction was cultured individually in either SC-islet medium [CMRL1066 (Corning, 15-110-CVR) plus 2 mM GlutaMAX, 2% Alburex20, 1:200 ITS-X, heparin (10 μg/ml), 10 μM zinc sulfate, 10 mM Hepes (Lonza, BEBP17-737E), nicotinamide (1.2 mg/ml; Apotheek AZL, 97996807), 0.5 mM sodium pyruvate (Lonza, BE13-115E), 1:2000 Trace Elements A (Corning, 25-021-CI), 1:2000 Trace Elements B (Corning, 99-175-CI), and 1:2000 lipid concentrate (Gibco, 11905-031)] or stage 7 medium (table S2) at 37°C in 5% CO_2 for 1 day before evaluation. Fractions 2 to 5 were pooled for some further analysis, mentioned as "enriched SC-islet." Fractions 1, 6, and 7 were pooled and mentioned as "depleted SC-islet."

Statistical analysis

Statistical analyses were performed using GraphPad Prism software. Data that passed the Shapiro-Wilk test for normal distribution were analyzed with parametric tests including Student's *t* test for comparison of two groups and analysis of variance (ANOVA) for comparison of more than two groups, as stated in each figure legend. Data that did not show normal distribution were analyzed with nonparametric tests including Wilcoxon (paired) and Mann-Whitney (nonpaired) tests for comparison of two groups and Friedman (paired) and Kruskal-Wallis (nonpaired) tests for comparison of more than two groups. $P < 0.05$ was considered statistically significant ($^*P < 0.05$, $^{**}P < 0.01$, $^{***}P < 0.001$).

Supplementary Materials

The PDF file includes:
Materials and Methods
Figs. S1 to S5
Tables S1 to S5
References (*49*–*57*)

Other Supplementary Material for this manuscript includes the following:
Data files S1 and S2
MDAR Reproducibility Checklist

REFERENCES AND NOTES

1. M.-C. Vantyghem, E. J. P. de Koning, F. Pattou, M. R. Rickels, Advances in β-cell replacement therapy for the treatment of type 1 diabetes. *Lancet* **394**, 1274–1285 (2019).
2. M. F. Nijhoff, M. A. Engelse, J. Dubbeld, A. E. Braat, J. Ringers, D. L. Roelen, A. R. van Erkel, H. S. Spijker, H. Bouwsma, P. J. M. van der Boog, J. W. de Fijter, T. J. Rabelink, E. J. P. de Koning, Glycemic stability through islet-after-kidney transplantation using an alemtuzumab-based induction regimen and long-term triple-maintenance immunosuppression. *Am. J. Transplant.* **16**, 246–253 (2016).
3. A. Rezania, J. E. Bruin, P. Arora, A. Rubin, I. Batushansky, A. Asadi, S. O'Dwyer, N. Quiskamp, M. Mojibian, T. Albrecht, Y. H. C. Yang, J. D. Johnson, T. J. Kieffer, Reversal of diabetes with insulin-producing cells derived in vitro from human pluripotent stem cells. *Nat. Biotechnol.* **32**, 1121–1133 (2014).
4. H. A. Russ, A. V. Parent, J. J. Ringler, T. G. Hennings, G. G. Nair, M. Shveygert, T. Guo, S. Puri, L. Haataja, V. Cirulli, R. Blelloch, G. L. Szot, P. Arvan, M. Hebrok, Controlled induction of human pancreatic progenitors produces functional beta-like cells in vitro. *EMBO J.* **34**, 1759–1772 (2015).
5. F. W. Pagliuca, J. R. Millman, M. Gurtler, M. Segel, A. Van Dervort, J. H. Ryu, Q. P. Peterson, D. Greiner, D. A. Melton, Generation of functional human pancreatic β cells in vitro. *Cell* **159**, 428–439 (2014).
6. N. J. Hogrebe, P. Augsornworawat, K. G. Maxwell, L. Velazco-Cruz, J. R. Millman, Targeting the cytoskeleton to direct pancreatic differentiation of human pluripotent stem cells. *Nat. Biotechnol.* **38**, 460–470 (2020).
7. V. Gorgogietas, B. Rajaei, C. Heeyoung, B. J. Santacreu, S. Marín-Cañas, P. Salpea, T. Sawatani, A. Musuaya, M. N. Arroyo, C. Moreno-Castro, K. Benabdallah, C. Demarez, S. Toivonen, C. Cosentino, N. Pachera, M. Lytrivi, Y. Cai, L. Carnel, C. Brown, F. Urano, P. Marchetti, P. Gilon, D. L. Eizirik, M. Cnop, M. Igoillo-Esteve, GLP-1R agonists demonstrate potential to treat Wolfram syndrome in human preclinical models. *Diabetologia* **66**, 1306–1321 (2023).
8. D. Balboa, T. Barsby, V. Lithovius, J. Saarimäki-Vire, M. Omar-Hmeadi, O. Dyachok, H. Montaser, P.-E. Lund, M. Yang, H. Ibrahim, A. Näätänen, V. Chandra, H. Vihinen, E. Jokitalo, J. Kvist, J. Ustinov, A. I. Nieminen, E. Kuuluvainen, V. Hietakangas, P. Katajisto, J. Lau, P.-O. Carlsson, S. Barg, A. Tengholm, T. Otonkoski, Functional, metabolic and transcriptional maturation of human pancreatic islets derived from stem cells. *Nat. Biotechnol.* **40**, 1042–1055 (2022).
9. F. Fantuzzi, S. Toivonen, A. A. Schiavo, H. Chae, M. Tariq, T. Sawatani, N. Pachera, Y. Cai, C. Vinci, E. Virgilio, L. Ladriere, M. Suleiman, P. Marchetti, J. C. Jonas, P. Gilon, D. L. Eizirik, M. Igoillo-Esteve, M. Cnop, In depth functional characterization of human induced pluripotent stem cell-derived beta cells in vitro and in vivo. *Front. Cell Dev. Biol.* **10**, 967765 (2022).
10. A. Veres, A. L. Faust, H. L. Bushnell, E. N. Engquist, J. H. Kenty, G. Harb, Y. C. Poh, E. Sintov, M. Gurtler, F. W. Pagliuca, Q. P. Peterson, D. A. Melton, Charting cellular identity during human in vitro beta-cell differentiation. *Nature* **569**, 368–373 (2019).
11. J. C. Davis, T. C. Alves, A. Helman, J. C. Chen, J. H. Kenty, R. L. Cardone, D. R. Liu, R. G. Kibbey, D. A. Melton, Glucose response by stem cell-derived beta cells in vitro is inhibited by a bottleneck in glycolysis. *Cell Rep.* **31**, 107623 (2020).
12. L. Velazco-Cruz, J. Song, K. G. Maxwell, M. M. Goedegebuure, P. Augsornworawat, N. J. Hogrebe, J. R. Millman, Acquisition of dynamic function in human stem cell-derived β cells. *Stem Cell Rep.* **12**, 351–365 (2019).
13. A. M. J. Shapiro, D. Thompson, T. W. Donner, M. D. Bellin, W. Hsueh, J. Pettus, J. Wilensky, M. Daniels, R. M. Wang, E. P. Brandon, M. S. Jaiman, E. J. Kroon, K. A. D'Amour, H. L. Foyt, Insulin expression and C-peptide in type 1 diabetes subjects implanted with stem cell-derived pancreatic endoderm cells in an encapsulation device. *Cell Rep. Med.* **2**, 100466 (2021).
14. T. W. Reichman, C. Ricordi, A. Naji, J. F. Markmann, B. A. Perkins, M. Wijkstrom, S. Paraskevas, B. Bruinsma, G. Marigowda, J. L. Shih, C. Wang, D. Melton, F. Pagliuca, B. Sanna, L. S. Kean, A. L. Peters, P. Witkowski, M. R. Rickels, 836-P: Glucose-dependent insulin production and insulin-independence in type 1 diabetes from stem cell–derived, fully differentiated islet cells—Updated data from the VX-880 clinical trial. *Diabetes* **72**, 836-P (2023).
15. European Medicines Agency, "Good manufacturing practice"; www.ema.europa.eu/en/human-regulatory-overview/research-development/compliance-research-development/good-manufacturing-practice.
16. J. Scherer, R. Seitz, Safety cell therapeutics/cell based medicinal products (CBMP). *Bundesgesundheitsbl.* **58**, 1199–1200 (2015).
17. J. L. Fowler, L. T. Ang, K. M. Loh, A critical look: Challenges in differentiating human pluripotent stem cells into desired cell types and organoids. *Wiley Interdiscip. Rev. Dev. Biol.* **9**, e368 (2020).
18. P. Augsornworawat, N. J. Hogrebe, M. Ishahak, M. D. Schmidt, E. Marquez, M. M. Maestas, D. A. Veronese-Paniagua, S. E. Gale, J. R. Miller, L. Velazco-Cruz, J. R. Millman, Single-nucleus multi-omics of human stem cell-derived islets identifies deficiencies in lineage specification. *Nat. Cell Biol.* **25**, 904–916 (2023).
19. P. U. Mahaddalkar, K. Scheibner, S. Pfluger, Ansarullah, M. Sterr, J. Beckenbauer, M. Irmler, J. Beckers, S. Knöbel, H. Lickert, Generation of pancreatic β cells from $CD177^+$ anterior definitive endoderm. *Nat. Biotechnol.* **38**, 1061–1072 (2020).
20. Y. Aghazadeh, F. Sarangi, F. Poon, B. Nkennor, E. C. McGaugh, S. S. Nunes, M. C. Nostro, GP2-enriched pancreatic progenitors give rise to functional beta cells in vivo and eliminate the risk of teratoma formation. *Stem Cell Rep.* **17**, 964–978 (2022).

21. K. F. Cogger, A. Sinha, F. Sarangi, E. C. McGaugh, D. Saunders, C. Dorrell, S. Mejia-Guerrero, Y. Aghazadeh, J. L. Rourke, R. A. Screaton, M. Grompe, P. R. Streeter, A. C. Powers, M. Brissova, T. Kislinger, M. C. Nostro, Glycoprotein 2 is a specific cell surface marker of human pancreatic progenitors. *Nat. Commun.* **8**, 331 (2017).
22. J. Ameri, R. Borup, C. Prawiro, C. Ramond, K. A. Schachter, R. Scharfmann, H. Semb, Efficient generation of glucose-responsive beta cells from isolated GP2$^+$ human pancreatic progenitors. *Cell Rep.* **19**, 36–49 (2017).
23. C. Ramond, N. Glaser, C. Berthault, J. Ameri, J. S. Kirkegaard, M. Hansson, C. Honoré, H. Semb, R. Scharfmann, Reconstructing human pancreatic differentiation by mapping specific cell populations during development. *eLife* **6**, e27564 (2017).
24. W. Jiang, X. Sui, D. Zhang, M. Liu, M. Ding, Y. Shi, H. Deng, CD24: A novel surface marker for PDX1-positive pancreatic progenitors derived from human embryonic stem cells. *Stem Cells* **29**, 609–617 (2011).
25. O. G. Kelly, M. Y. Chan, L. A. Martinson, K. Kadoya, T. M. Ostertag, K. G. Ross, M. Richardson, M. K. Carpenter, K. A. D'Amour, E. Kroon, M. Moorman, E. E. Baetge, A. G. Bang, Cell-surface markers for the isolation of pancreatic cell types derived from human embryonic stem cells. *Nat. Biotechnol.* **29**, 750–756 (2011).
26. K. Molakandov, D. A. Berti, A. Beck, O. Elhanani, M. D. Walker, Y. Soen, K. Yavriyants, M. Zimerman, E. Volman, I. Toledo, A. Erukhimovich, A. M. Levy, A. Hasson, J. Itskovitz-Eldor, J. Chebath, M. Revel, Selection for CD26$^-$ and CD49A$^+$ cells from pluripotent stem cells-derived islet-like clusters improves therapeutic activity in diabetic mice. *Front. Endocrinol.* **12**, 635405 (2021).
27. D. C. Saunders, M. Brissova, N. Phillips, S. Shrestha, J. T. Walker, R. Aramandla, G. Poffenberger, D. K. Flaherty, K. P. Weller, J. Pelletier, T. Cooper, M. T. Goff, J. Virostko, A. Shostak, E. D. Dean, D. L. Greiner, L. D. Shultz, N. Prasad, S. E. Levy, R. H. Carnahan, C. Dai, J. Sevigny, A. C. Powers, Ectonucleoside triphosphate diphosphohydrolase-3 antibody targets adult human pancreatic β cells for in vitro and in vivo analysis. *Cell Metab.* **29**, 745–754.e4 (2019).
28. F. M. Docherty, K. A. Riemondy, R. Castro-Gutierrez, J. M. Dwulet, A. H. Shilleh, M. S. Hansen, S. P. M. Williams, L. H. Armitage, K. E. Santostefano, M. A. Wallet, C. E. Mathews, T. M. Triolo, R. K. P. Benninger, H. A. Russ, ENTPD3 marks mature stem cell–derived β-cells formed by self-aggregation in vitro. *Diabetes* **70**, 2554–2567 (2021).
29. A. V. Parent, S. Ashe, G. G. Nair, M. L. Li, J. Chavez, J. S. Liu, Y. Zhong, P. R. Streeter, M. Hebrok, Development of a scalable method to isolate subsets of stem cell-derived pancreatic islet cells. *Stem Cell Rep.* **17**, 979–992 (2022).
30. J. C. Davis, A. Helman, J. Rivera-Feliciano, C. M. Langston, E. N. Engquist, D. A. Melton, Live cell monitoring and enrichment of stem cell-derived β cells using intracellular zinc content as a population marker. *Curr. Protoc. Stem Cell Biol.* **51**, e99 (2019).
31. G. G. Nair, J. S. Liu, H. A. Russ, S. Tran, M. S. Saxton, R. Chen, C. Juang, M.-L. Li, V. Q. Nguyen, S. Giacometti, S. Puri, Y. Xing, Y. Wang, G. L. Szot, J. Oberholzer, A. Bhushan, M. Hebrok, Recapitulating endocrine cell clustering in culture promotes maturation of human stem-cell-derived β cells. *Nat. Cell Biol.* **21**, 263–274 (2019).
32. F. C. Wieland, M. M. J. P. E. Sthijns, T. Geuens, C. A. van Blitterswijk, V. L. S. LaPointe, The role of alpha cells in the self-assembly of bioengineered islets. *Tissue Eng. Part A* **27**, 1055–1063 (2021).
33. Y. H. Jo, I. J. Jang, J. G. Nemeno, S. Lee, B. Y. Kim, B. M. Nam, W. Yang, K. M. Lee, H. Kim, T. Takebe, Y. S. Kim, J. I. Lee, Artificial islets from hybrid spheroids of three pancreatic cell lines. *Transplant. Proc.* **46**, 1156–1160 (2014).
34. C. Kelly, H. G. Parke, J. T. McCluskey, P. R. Flatt, N. H. McClenaghan, The role of glucagon- and somatostatin-secreting cells in the regulation of insulin release and beta-cell function in heterotypic pseudoislets. *Diabetes-Metab. Res. Rev.* **26**, 525–533 (2010).
35. F. C. Wieland, C. A. van Blitterswijk, A. van Apeldoorn, V. L. S. LaPointe, The functional importance of the cellular and extracellular composition of the islets of Langerhans. *J. Immunol. Regen. Med.* **13**, 100048 (2021).
36. C. A. Cowan, I. Klimanskaya, J. McMahon, J. Atienza, J. Witmyer, J. P. Zucker, S. P. Wang, C. C. Morton, A. P. McMahon, D. Powers, D. A. Melton, Derivation of embryonic stem-cell lines from human blastocysts. *N. Engl. J .Med.* **350**, 1353–1356 (2004).
37. P. A. De Sousa, B. J. Tye, K. Bruce, P. Dand, G. Russell, D. M. Collins, A. Greenshields, K. McDonald, H. Bradburn, M. A. Canham, T. Kunath, J. M. Downie, M. Bateman, A. Courtney, Derivation of the clinical grade human embryonic stem cell line RCe013-A (RC-9). *Stem Cell Res.* **17**, 36–41 (2016).
38. J. J. Novoa, I. M. Westra, E. Steeneveld, N. Fonseca Neves, C. H. Arendzen, B. Rajaei, E. Grundeken, M. Yildiz, W. van der Valk, A. Salvador, F. Carlotti, P. F. Dijkers, H. Locher, C. W. van den Berg, K. I. Raymond, A. Kirkeby, C. L. Mummery, T. J. Rabelink, C. Freund, P. Meij, B. Wieles, Good Manufacturing Practice-compliant human induced pluripotent stem cells: From bench to putative clinical products. *Cytotherapy* **26**, 556–566 (2024).
39. J. Novoa, I. Westra, E. Steeneveld, N. F. Neves, L. Daleman, A. B. Asensio, R. P. Davis, F. Carlotti, C. Freund, T. Rabelink, P. Meij, B. Wieles, Validating human induced pluripotent stem cell-specific quality control tests for the release of an intermediate drug product in a Good Manufacturing Practice quality system. *Cytotherapy* **26**, 1105–1117 (2024).
40. J. B. Doppenberg, M. F. Nijhoff, M. A. Engelse, E. J. P. de Koning, Clinical use of donation after circulatory death pancreas for islet transplantation. *Am. J. Transplant.* **21**, 3077–3087 (2021).
41. L. van Gurp, L. Fodoulian, D. Oropeza, K. Furuyama, E. Bru-Tari, A. N. Vu, J. S. Kaddis, I. Rodríguez, F. Thorel, P. L. Herrera, Generation of human islet cell type-specific identity genesets. *Nat. Commun.* **13**, 2020 (2022).
42. J. B. Doppenberg, M. A. Engelse, E. J. P. de Koning, PRISM: A novel human islet isolation technique. *Transplantation* **106**, 1271–1278 (2022).
43. M. D. Schmidt, M. Ishahak, P. Augsornworawat, J. R. Millman, Comparative and integrative single cell analysis reveals new insights into the transcriptional immaturity of stem cell-derived β cells. *BMC Genomics* **25**, 105 (2024).
44. S. P. Lake, P. D. Bassett, A. Larkins, J. Revell, K. Walczak, J. Chamberlain, G. M. Rumford, N. J. M. London, P. S. Veitch, P. R. F. Bell, R. F. L. James, Large-scale purification of human islets utilizing discontinuous albumin gradient on IBM-2991 cell separator. *Diabetes* **38**, 143–145 (1989).
45. A. R. Pepper, A. Bruni, R. Pawlick, D. O'Gorman, T. Kin, A. Thiesen, A. M. J. Shapiro, Posttransplant characterization of long-term functional hESC-derived pancreatic endoderm grafts. *Diabetes* **68**, 953–962 (2019).
46. V. Lithovius, S. Lahdenpohja, H. Ibrahim, J. Saarimäki-Vire, L. Uusitalo, H. Montaser, K. Mikkola, C.-B. Yim, T. Keller, J. Rajander, D. Balboa, T. Barsby, O. Solin, P. Nuutila, T. J. Grönroos, T. Otonkoski, Non-invasive quantification of stem cell-derived islet graft size and composition. *Diabetologia* **67**, 1912–1929 (2024).
47. H. Zhu, G. Wang, K.-V. Nguyen-Ngoc, D. Kim, M. Miller, G. Goss, J. Kovsky, A. R. Harrington, D. C. Saunders, A. L. Hopkirk, R. Melton, A. C. Powers, S. Preissl, F. M. Spagnoli, K. J. Gaulton, M. Sander, Understanding cell fate acquisition in stem-cell-derived pancreatic islets using single-cell multiome-inferred regulomes. *Dev. Cell* **58**, 727–743.e11 (2023).
48. K. Furuyama, S. Chera, L. van Gurp, D. Oropeza, L. Ghila, N. Damond, H. Vethe, J. A. Paulo, A. M. Joosten, T. Berney, D. Bosco, C. Dorrell, M. Grompe, H. Ræder, B. O. Roep, F. Thorel, P. L. Herrera, Diabetes relief in mice by glucose-sensing insulin-secreting human α-cells. *Nature* **567**, 43–48 (2019).
49. H. S. Spijker, R. B. G. Ravelli, A. M. Mommaas-Kienhuis, A. A. van Apeldoorn, M. A. Engelse, A. Zaldumbide, S. Bonner-Weir, T. J. Rabelink, R. C. Hoeben, H. Clevers, C. L. Mummery, F. Carlotti, E. J. P. de Koning, Conversion of mature human β-cells into glucagon-producing α-cells. *Diabetes* **62**, 2471–2480 (2013).
50. F. G. A. Faas, M. C. Avramut, B. M. van den Berg, A. M. Mommaas, A. J. Koster, R. B. G. Ravelli, Virtual nanoscopy: Generation of ultra-large high resolution electron microscopy maps. *J. Cell Biol.* **198**, 457–469 (2012).
51. N. R. Johnston, R. K. Mitchell, E. Haythorne, M. P. Pessoa, F. Semplici, J. Ferrer, L. Piemonti, P. Marchetti, M. Bugliani, D. Bosco, E. Berishvili, P. Duncanson, M. Watkinson, J. Broichhagen, D. Trauner, G. A. Rutter, D. J. Hodson, Beta cell hubs dictate pancreatic islet responses to glucose. *Cell Metab.* **24**, 389–401 (2016).
52. L. van der Maaten, G. Hinton, Visualizing data using t-SNE. *J. Mach. Learn. Res.* **9**, 2579–2605 (2008).
53. R. Satija, J. A. Farrell, D. Gennert, A. F. Schier, A. Regev, Spatial reconstruction of single-cell gene expression data. *Nat. Biotechnol.* **33**, 495–502 (2015).
54. M. J. Muraro, G. Dharmadhikari, D. Grün, N. Groen, T. Dielen, E. Jansen, L. van Gurp, M. A. Engelse, F. Carlotti, E. J. de Koning, A. van Oudenaarden, A single-cell transcriptome atlas of the human pancreas. *Cell Syst.* **3**, 385–394.e3 (2016).
55. H. Wickham, ggplot2. *WIREs Comput. Stat.* **3**, 180–185 (2011).
56. D. Grün, A. Lyubimova, L. Kester, K. Wiebrands, O. Basak, N. Sasaki, H. Clevers, A. van Oudenaarden, Single-cell messenger RNA sequencing reveals rare intestinal cell types. *Nature* **525**, 251–255 (2015).
57. V. A. Traag, L. Waltman, N. J. van Eck, From Louvain to Leiden: Guaranteeing well-connected communities. *Sci. Rep.* **9**, 5233 (2019).

Acknowledgments: We thank M. Hanegraaf, N. de Jong, E. Steeneveld, M. Ajie, and A. Verpoorte (all from LUMC, Department of Internal Medicine) for expert technical support. We are grateful to A. L. Roelofsen, B. Brinkhof (LUMC, Department of Internal Medicine), and P. Meij (LUMC, Department of Center for Cell and Gene Therapy) and E. van der Stoep-Yap (LUMC, Department of Clinical Pharmacy and Toxicology) for, respectively, contributing in making and validating the cell bank of clinical-grade RC9 in the GMP facility of our institute. We thank B. Wieles (LUMC, Department of Internal Medicine) for providing the LUMC iPSC lines. We thank C. Jost and R. Koning (LUMC, Department of Cell and Chemistry Biology) for helpful discussion on the analysis of the electron microscopy images. We thank M. Ajie (LUMC, Department of Internal Medicine) for bioinformatics support. We thank M. Zuurmond (LUMC, Department of Internal Medicine) for the illustration of the schematic figures. **Funding:** This research was supported by the RegMedXB consortium, the DON Foundation, the Dutch Diabetes Research Foundation, the Bontius Foundation, and the Novo Nordisk Foundation Center for Stem Cell Medicine reNEW (NNF21CC0073729). **Author contributions:** B.R., F.C., and E.J.P.d.K. conceptualized the study. B.R., J.B.D., M.A.E., E.J.P.d.K., and F.C. developed the methodology. B.R., M.P.-B., F.B., A.A.M., F.L., L.D., A.E.d.L., M.C.N., and W.d.V. performed experiments. A.M.G. and J.J. contributed to bioinformatics analysis. T.R. provided resources. F.C. and E.J.P.d.K. supervised the study and acquired funding. B.R. wrote the original draft. B.R. and F.C. edited the revised

final draft of the study. **Competing interests:** B.R., J.B.D., M.A.E., E.J.P.d.K, and F.C. are named as inventors on a patent (Enrichment or isolation of cell clusters, PCT/NL2024/050604) related to the content of this manuscript. E.J.P.d.K. is a councillor for the International Pancreas and Islet Transplantation Association and an advisor for Evotec, Novo Nordisk, Vertex, and Zurich Transplantation Center. The other authors declare that they have no competing interests. **Data and materials availability:** All data associated with this study are present in the paper or the Supplementary Materials. Single-cell RNA sequencing data can be accessed at the European Genome-Phenome Archive (EGA): accession EGAS50000000905. Human pluripotent stem cell lines were obtained under material transfer agreements [HUES8 (WiCell), RC9 (Roslin), and LUMC iPSC (LUMC)]. Data file S1 contains raw data from all figures. Data file S2 contains the lists of differentially expressed genes for each cluster presented in Fig. 4, I and J.

Submitted 8 November 2023
Resubmitted 28 August 2024
Accepted 10 March 2025
Published 2 April 2025
10.1126/scitranslmed.adl4390

Science Translational Medicine

Clinically compliant enrichment of human pluripotent stem cell–derived islets

Bahareh Rajaei, Amadeo Muñoz Garcia, Juri Juksar, Jason B. Doppenberg, Miriam Paz-Barba, Fransje Boot, Willemijn de Vos, Aat A. Mulder, Ferdy Lambregtse, Lizanne Daleman, Anne E. de Leeuw, Maaike C. Nieveen, Marten A. Engelse, Ton Rabelink, Eelco J. P. de Koning, and Françoise Carlotti

Sci. Transl. Med. **17** (792), eadl4390. DOI: 10.1126/scitranslmed.adl4390

Editor's summary

Stem cell–derived pancreatic islets are being investigated as a possible therapy for type 1 diabetes. Such # cell replacement therapies would require large numbers of stem cell–derived endocrine cells produced according to clinical standard manufacturing practices. Rajaei *et al*. developed a protocol that uses density gradient centrifugation to enrich target endocrine cell clusters while reducing the number of undesired, incorrectly differentiated cells. The cell clusters further matured after transplantation into immunodeficient mice, showed signs of functionality, and remained viable at 6 months posttransplantation. This study supports further functional and safety testing of this methodology in the context of type 1 diabetes–directed regenerative therapies, including testing in diabetic animals. —Catherine Charneski

Science Translational Medicine (ISSN 1946-6242) is published by the American Association for the Advancement of Science. 1200 New York Avenue NW, Washington, DC 20005. The title *Science Translational Medicine* is a registered trademark of AAAS.